Effectiveness of Disulfide Bridged Cyclic Peptide as AFB1 Mimotope

by

Jake Simmons

Submitted to the Board of Chemistry
School of Natural and Social Sciences
In partial fulfillment of the requirements
For the Degree of Bachelor of Arts

Purchase College
State University of New York

May 2021

Sponsor: Dr. Elizabeth Middleton

Second Reader: Dr. Joe Skrivanek

Introduction

Aflatoxins are toxic, carcinogenic, and mutagenic molecules produced by fungi of the species *Aspergillus flavus* and *Aspergillus parasiticus.* They fall under the category of mycotoxins, or toxins produced by fungi, but are perhaps the most significant of the mycotoxins due to the fact that the fungi that produce them are common contaminants in several food products, such as corn, animal feed, and peanuts. As a result, development of methods for detecting small quantities of aflatoxin contamination in food is of the utmost importance, especially for application in more tropical areas of the world where the fungi grow more readily. In general, aflatoxin exposure has been shown to cause many different types of cancer, most commonly liver cancer but also cancer of the kidney, pancreas, skin, and lungs. Aflatoxins also have immunosuppressant, genotoxic, and mutagenic effects, and are linked to certain nutritional disorders such as kwashiorkor, a malnutrition based condition caused by poor protein intake (Benkerroum, 2020).

Of the eighteen aflatoxins that are known to exist, only six have been deemed to be of scientific importance; B_1, B_2, G_1, G_2, M_1, and M_2. Of these six, aflatoxin B_1, or AFB1, is by far the most hazardous, the most common (accounting for 75% of all aflatoxin contamination), and the most extensively studied (Wacoo, 2014). There are two primary paths by which AFB1 enacts its

toxicity once inside the body; conversion into AFB1-exo 8,9-epoxide, and through oxidative stress, which is produced as a byproduct of the former reaction. Though AFB1-exo 8,9-epoxide, or AFBO, has been thought to be the primary cause of AFB1 toxicity, there is increasing data suggesting that oxidative stress plays a far greater role than previously believed (Benkerroum, 2020).

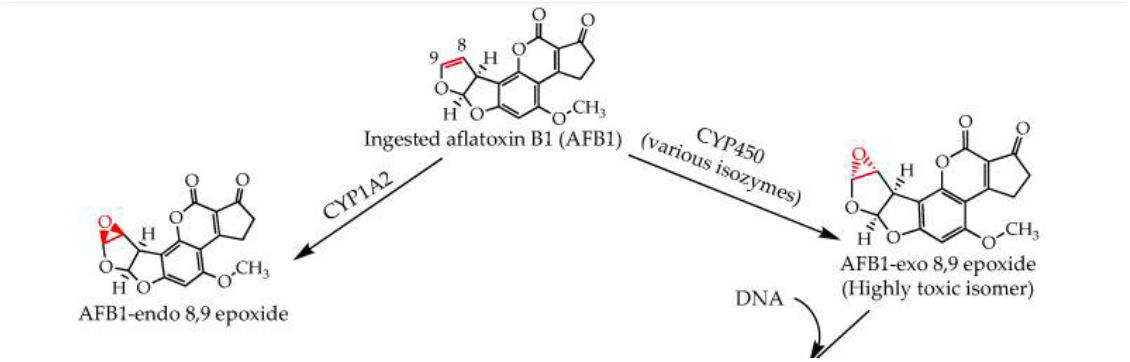

Figure 1; The structure of AFB1 is shown, in addition to AFBO on the right, and the far less toxic isomer AFB1-endo 8,9 epoxide on the left. (Benkerroum, 2020)

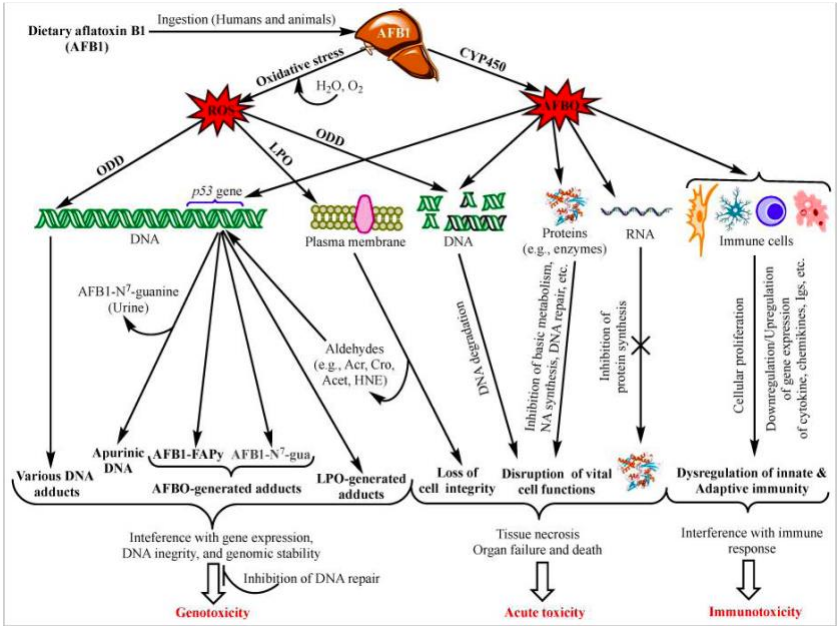

Figure 2; Mechanisms of action of AFB1. At the top of the chart, the two main pathways of AFB1 toxicity can be seen; Conversion to AFBO by CYP3a4 on the right, and oxidative stress released from the conversion to AFBO on the left. The various ways in which damage is caused by these two pathways is outlined. (Benkerroum, 2020)

AFB1 is metabolized mostly in the liver and primarily by one of two enzymes, CYP1a2 or CYP3a4, both belonging to a group of microsomal cytochrome enzymes known as CYP450. The activity of each enzyme varies depending on the amount of AFB1 being metabolized. In low doses, CYP1a2 is the dominant enzyme in metabolism and primarily produces AFB1-endo 8,9-epoxide, a significantly less toxic isomer of AFBO. In large doses, CYP3a4 is the dominant enzyme, and produces primarily AFBO. Once AFBO is released, it covalently bonds with DNA, most commonly with codon 249 of the p53 tumor suppressor gene, and induces an AGG → AGT transversion point mutation. This causes proteins to be expressed that cannot properly bind to target DNA, and therefore lose their capacity to signal or transactivate vital cell functions such as cell cycle arrest and apoptosis, damaging the body's ability to halt the growth of tumors. This eventually leads to various forms of cancer (Benkerroum, 2020).

Cytochrome P450 3a4 is a liver enzyme that is involved in the metabolism of a majority of drugs. It is a homodimer and contains identical subunits divided into two sections; one N-terminal domain containing many β-sheets, and one C-terminal domain containing many α-helices in addition to the active site (Nyenhuis). CYP3a4 is capable of having two or more molecules in its active site at one time, allowing it to facilitate drug-drug interactions. It can also oxidize bound substrates due to the presence of a HEME group bordering the active site. CYP3a4 can inhibit the effectiveness of drugs by metabolizing them soon after they enter the body, specifically HIV protease inhibitors. To combat this, ritonavir can be administered to strongly inhibit the function of CYP3a4. The active site of CYP3a4 is located within the molecule

itself, and is not immediately accessible from the outside. A conformational shift of CYP3a4 is required for a ligand to enter and bind to the active site (Sevrioukova, 2013).

Figure 3; 3D model of CYP3a4. Left and right are the two identical subunits. Within each, a colored ligand can be seen in the respective active sites. "Cytochrome P450 3A4 homodimer + 2 HEM (green-red) + 2 D7J inhibitor (l.blue-red), Human" https://en.wikipedia.org/wiki/CYP3A4#/media/File:6bd7.jpg

When AFB1 is metabolized into AFBO in the liver, oxidative stress is produced. Oxidative stress, or OS, refers to the damage inflicted on a biological system by an uncontrolled quantity of reactive oxygen species. The metabolism of AFB1 produces these reactive oxygen species which, like AFBO, can form adducts with DNA and cause lesions. In addition to this, they also inflict lipid peroxidation on cell membranes, which can produce many different mutagenic aldehydes, such as malondialdehyde, acrolein, 4-hydroxy-2-nonenal, and 4-oxo-2(E)-nonenal. These aldehydes can then form a wide variety of mutagenic DNA adducts leading to further

potential for mutagenesis and carcinogenesis. Recent data suggests that the role that oxidative stress plays in AFB1 toxicity is greater than previously suspected (Benkerroum, 2020).

AFB1 is incredibly hazardous, so many precautions must be taken prior to handling any samples of the toxin in a laboratory setting. This involves at the very least the use of gloves, a face shield, and a respirator. Due to this, there is incentive to research non-toxic AFB1 mimotopes. A mimotope is a molecule that imitates the structure of another molecule, causing an antibody (or antibodies) to bind to it the same way that it would bind to the original molecule. Levels of AFB1 contamination in food products are often very small, so to detect these trace amounts, a competitive ELISA is commonly used. In a competitive ELISA, antibodies against the target antigen are attached to testing plates and are made to bind to a competitive antigen which has been labeled with biotin. The sample containing the target antigen is then run over the testing plates and the target antigen binds to the antibodies in place of the competitive antigen. Due to the fact that only the competitive antigen was bound to biotin, the remaining quantity of competitive antigen present in the testing wells can then be revealed by testing for the quantity of biotin, which would in turn reveal the quantity the competitive antigen that was displaced by the target antigen. From this, one could figure out the quantity of target antigen in the sample. One research paper (Mukhtar, H., 2019) managed to identify a cyclic peptide that functions as an effective AFB1 mimotope. This was done because one of the most commonly used competitive antigens for AFB1 is AFB1-OVA/AFB1-BSA, a derivative of AFB1 that requires handling of AFB1 to produce. The cyclic peptide discovered by this paper can be safely and easily synthesized in a laboratory without requiring any AFB1 exposure, making it

very useful as an alternative competitive antigen for development of AFB1 detection tests (Mukhtar, H., 2019).

To discover the cyclic peptide, a disulfide-cyclized Ph.D.-C7C phage display library was biopanned using anti-AFB1 MAb 2F5 bound to testing wells. A phage display library like this is a collection of cyclic peptides bound to phage particles, which can be biopanned using antibodies of interest, in this case mAb 2F5, to isolate specific peptides that have good binding affinity towards the antibody. Peptides that bound to MAb 2F5 were isolated and their binding strength was evaluated. The peptide that was selected for use in the experiment had the structure CVPSKPGLC, and it was selected due to the quality of its binding affinity with mAb 2F5. After identifying the peptide, it was chemically synthesized, biotinylated, and used in a biotinylated peptide ELISA. The bp-ELISA was then used to find the AFB1 concentration from samples of rice and corn spiked with known concentrations of AFB1. The results of these tests showed that the average recovery of AFB1 by bp-ELISA was 84-97% in samples of rice and 83-102% in samples of corn. Experiments were also carried out to determine how specific the test is for AFB1 detection. It was shown that the bp-ELISA is highly specific for AFB1 and only very slightly (<0.1% - <1.0%) cross reactive with similar toxins AFB2, AFG1, AFG2, ZEN, OTA, and CIT. These results indicate that the cyclic peptide functions very well as a competitive antigen for AFB1, and that the bp-ELISA is efficient and viable for real-world applications (Mukhtar, H., 2019).

The goal of this project is to use computer modeling to simulate the interaction between the cyclic peptide identified by Mukhtar and two known and biologically significant AFB1 binding partners, MAb 2F5 and CYP3a4, and compare that to the interactions between

the same antibodies and AFB1. The purpose of these dockings is to evaluate how effective of an AFB1 mimotope the cyclic peptide is outside of the context of a bp-ELISA. Additionally, the simulations will be analyzed to determine similarities between the docks of AFB1 and the cyclic peptide. This will be done to try and determine the specific structural components of the cyclic peptide that are meant to mimic AFB1.

Several computer programs will be used in this experiment for modeling and docking purposes. The online program PEP-FOLD 3.5 will be used to produce a 3d model of the linear peptide, and PEP-Cyclizer will be used to cyclize the peptide with a disulfide bridge. These programs are both available for free and can be used in-browser. The program Chimera will be used for the loading and manipulation of all 3d models. Chimera alone is very useful for analyzing molecules, and comes with a wide variety of tools to assist in the visualization of complex molecules, but on its own it cannot dock molecules together. For this, the program Autodock Vina will be used. Autodock Vina is compatible with Chimera, and can be loaded as an add-on in the program. All of the docking will be done by Autodock Vina, but the setup and results will be visible through Chimera.

The two molecules that were selected for binding, MAb 2F5 and CYP3a4, were selected for specific reasons. CYP3a4 was selected due to the important role it plays in the metabolism of AFB1. It is the enzyme that converts AFB1 into AFBO, and is one of the only enzymes in the body that AFB1 interacts with. It is also a well-known and widely studied enzyme, meaning that CYP3a4 molecular models and other general information is not hard to come by. MAb 2F5 was selected because it an anti-AFB1 antibody which was used in the Mukhtar article to biopan the phage library for AFB1 mimotopes. Since it is known that the cyclic peptide should bind with the

antibody, it would be useful to compare the strength and types of interactions of the cyclic peptide's bond to those of AFB1.

Methods

Preparation of 3D Models

Before the experiment was carried out, the 3d models for each molecule used had to be downloaded and prepared for docking. The online program PEP-FOLD (https://mobyle.rpbs.univ-paris-diderot.fr/cgi-bin/portal.py#forms::PEP-FOLD3) was used to create a 3d model of the linear peptide CVPSKPGLC. Default settings were used. The following input was used to generate the model:

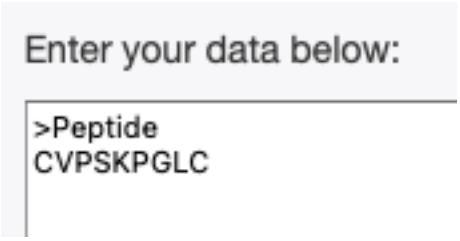

Figure 4; PEP-FOLD 3.5 input settings.

Using the 3d model of the linear peptide and the website https://bioserv.rpbs.univ-paris-diderot.fr/services/PEP-Cyclizer/#problems , a 3d model of the disulfide bridged peptide was created. For this, the 3d model of the linear peptide was uploaded to the website and cyclized. AFB1 model with chemspider.com id 162470, mAb 2F5 model "3idg" and CYP3a4 models

"4D7D," "4D75," "5A1R," "5VC0," and "1TQN" were downloaded. Ligands and solvent from each CYP3a4 model and the mAb 2F5 model were removed. In Chimera, all of the ligand and receptor models were dock prepped. For all dock preps, the following settings were used:

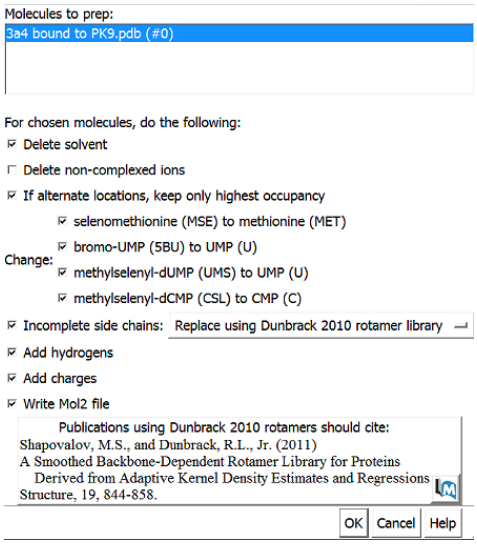

Figure 5; Dock prep settings screen 1.

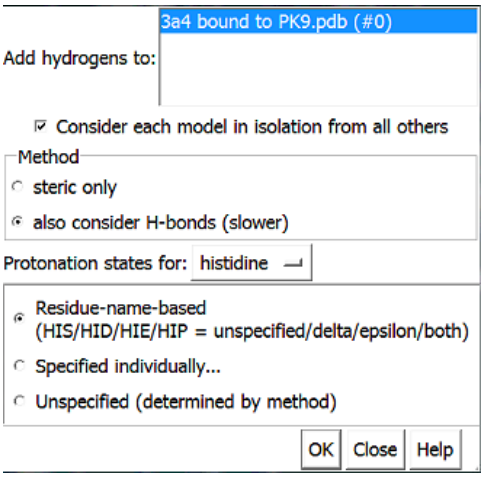

Figure 6; Dock prep settings screen 2.

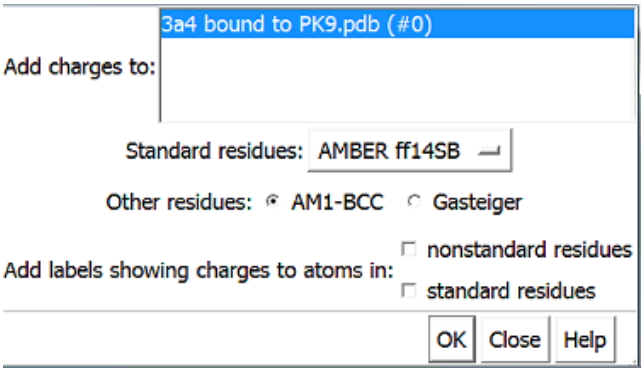

Figure 7; Dock prep settings screen 3.

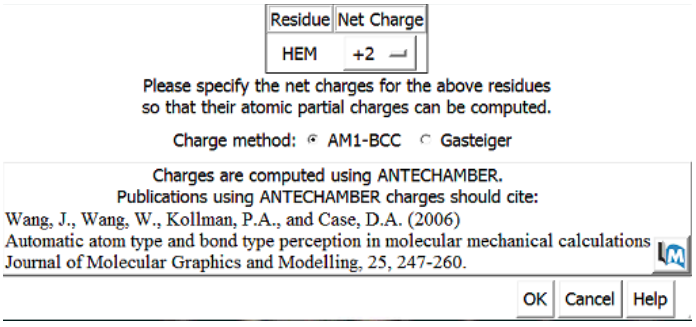

Figure 8; Dock prep settings screen 4.

After dock prep was completed, AFB1 and cyclic peptide models were minimized. Default settings for minimization except for “conjugate gradient steps,” which was set to 10,000 to ensure model was fully minimized.

Molecular Docking

Once the 3d molecules of each molecule were obtained, the process of docking them together could begin. The Autodock tool was used to simulate a docking of each ligand to each receptor. The following parameters were used for each autodock.

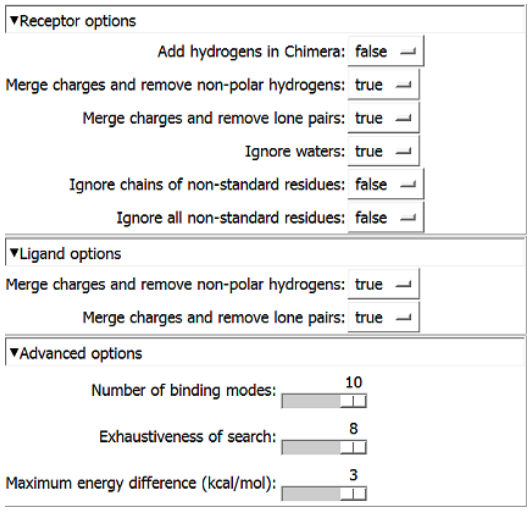

Figure 9; Autodock settings.

In addition, the following inputs for the search volume were used for each receptor to ensure the active site was completely encased.

- *CYP3a4 bound to PKT:* Center (-22.72, 22.65, 10.67) Size (23.91, 28.73, 30.44).
- *CYP3a4 bound to PK9:* Center (-22.64, -20.30, -10.36) Size (21.48, 29.03, 26.19).

- *CYP3a4 bound to Progesterone:* Center (-22.76, -21.25, -10.02) Size (22.08, 32.16, 29.56).
- *CYP3a4 bound to Ritonavir:* Center (36.59, -20.26, 26.69) Size (24.74, 26.87, 21.98).
- *Empty CYP3a4:* Center (-23.07, -21.28, -11.72) Size (22.07, 28.52, 23.74).
- *mAb 2F5:* Center (6.85, 51.22, 87.65) Size (66.29, 48.52, 50.15).

For each autodock, the first result in the list of best docks was recorded.

Active Site Analysis

Once the docks were all comleted, analysis of the results could begin. In addition to analysis of docking results, the dimensions of the active site of each model of CYP3a4 were also measured and analyzed to determine trends with active site size and cyclic peptide binding affinity. The openness of the active site was evaluated for each CYP3a4 model by measuring the distance between several atoms around the active site. To do this, two atoms were selected, and the "Distances" tool was used to draw a line between them. Distance was recorded in Angstroms. The following atoms were used to function as the limits of each dimension of the active site:

- Y Dimension: :213@CZ and HEM@FE
- X Dimension: :305@CB and :370@CB
- Z Dimension: :119@OG and :309@OG1

X, Y, and Z distances for each model of CYP3a4 were added and multiplied to obtain values representing approximate active site openness. For each CYP3a4 model, a chart was prepared displaying the active site dimensions, the product of the active site dimensions, the best dock for the cyclic peptide, and the best dock for AFB1.

Results

The correlation between peptide dock strength and active site openness was graphed in figures 1 and 2. One graph was made with the sum of the active site dimensions, and one was made with the product of the active site dimensions. The R^2 values indicate that there is a stronger positive correlation to dock strength with the product of the active site dimensions versus the sum of the active site dimensions. This means that, assuming active site openness is the primary determinant of peptide dock strength, the product of the active site dimensions should be a more accurate figure to represent the openness of the active site. This is because the product of the three axes gives the volume of a rectangular approximation of the active site.

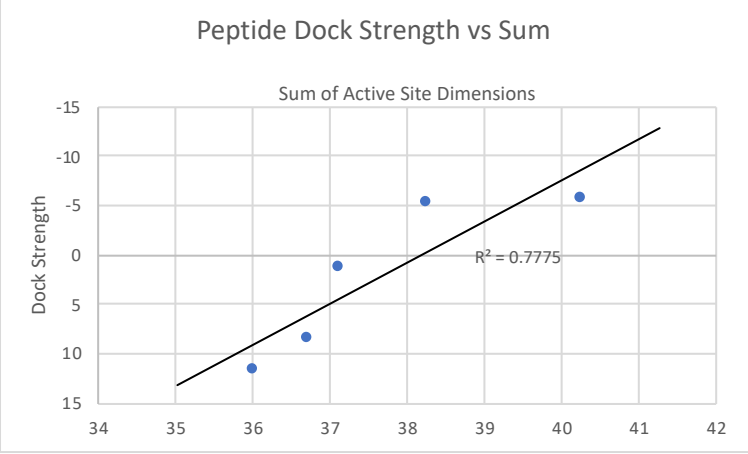

Figure 10; Graph of Peptide Dock Strength vs. Sum of Active Site Dimensions. R^2 value calculated to be 0.7775.

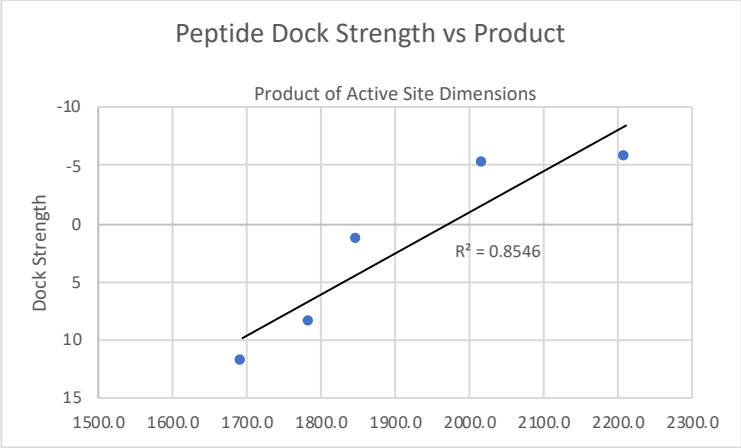

Figure 11; Graph of Peptide Dock Strength vs. Product of Active Site Dimensions. R^2 value calculated to be 0.8546.

Three atomic distances were measured to function as the x, y, and z dimensions of each CYP3a4 active site. The atoms were selected based off of a visual examination of the active site, and due to the fact that they did not move in relation to each other very much between different CYP3a4 models and remained good markers, despite the changing in active site size. The atoms used for each dimension are as follows; :305@CB and :370@CB for the X axis, :213@CZ and HEM@FE for the Y axis, and :119@OG and :309@OG1 for the Z axis. The first number after the colon represents the residue number of the amino acid. Following the "@" symbol is the atom name, where the first value is the atom type, the second value represents the remoteness from the carbonyl carbon of the amino acid, and the third value represents the branch number in scenarios where there are more than one of the same atom bound to the same carbon. In the following images, the X axis is displayed as the line between the two blue atoms, the Y axis is the line between the two yellow atoms, and the Z axis is the line between the two red atoms. Figure 12 shows the active site in relation to the rest of the molecule, while figure 13 shows the active site dimensions from the same perspective but without the rest of the molecule present.

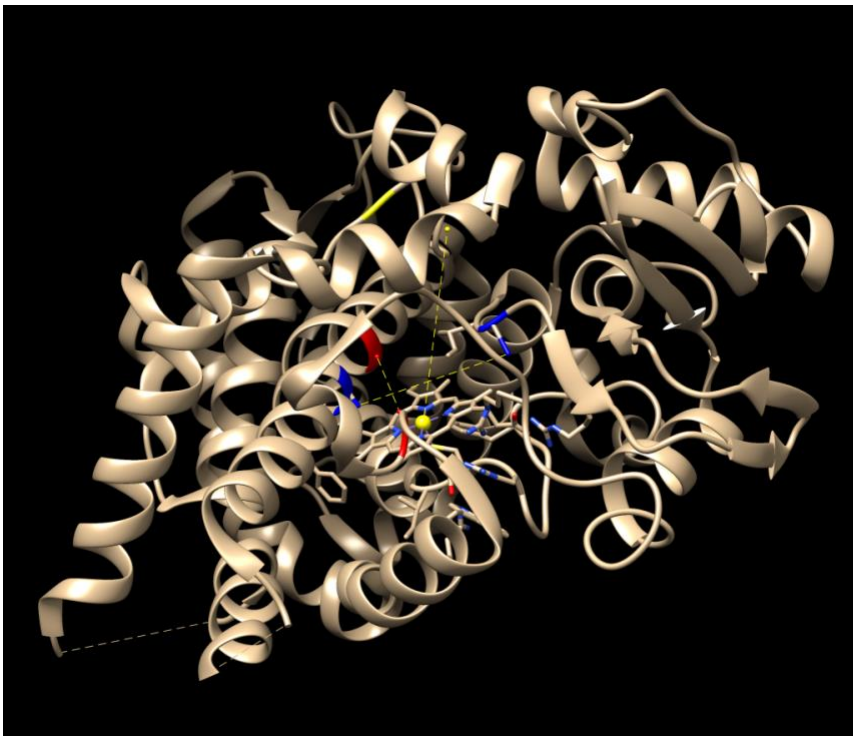

Figure 12; CYP3a4 model with active site dimensions drawn.

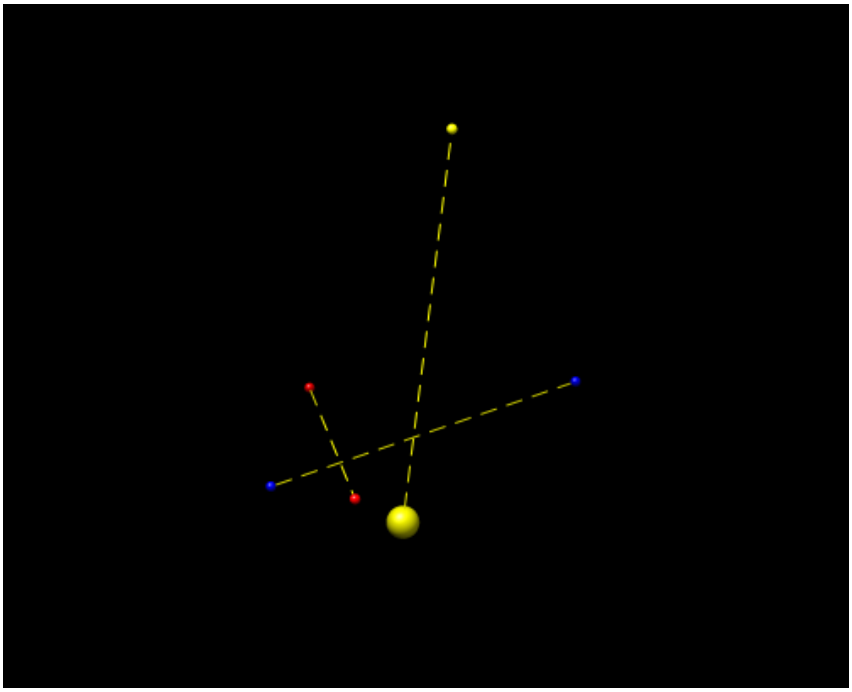

Figure 13; Active site dimensions from figure 12 with the rest of the molecule hidden.

The cyclic peptide and AFB1 were docked with multiple models of enzyme CYP3a4. The results of the docking of the cyclic peptide and AFB1 with each model of CYP3a4 are organized in Table 1, along with the measured dimensions of the active site of each model of CYP3a4. CYP3a4 models are named based off of the ligand they were originally bound with when the 3d models were obtained via x-ray diffraction. The different sizes of these original ligands resulted in different CYP3a4 active site dimensions, which were shown to greatly affect the cyclic peptide's ability to dock. For the active site dimensions, the x, y, and z dimensions were both added and multiplied in an effort to determine the best single number to represent the active site openness of each model.

For the docking results, the dock strength value represents the free energy of the molecule, therefore a lower number is preferable and indicates a stronger dock. The units for these values are kcal/mol. From this data, it is clear that the CYP3a4 models with ligands Ritonavir and PKT were the most well suited for docking with the cyclic peptide. These two models also reported the largest active site openness, both in the sum of the active site dimensions and the product. All models of CYP3a4 seemed to be well suited for docking with AFB1 with little variance between models and a range of only 1.3, compared to the cyclic peptide's range of 16.9. For docks, a score above zero means that there is an increase in energy of the system due to the bond, meaning it is unlikely to occur in the real world.

CYP3a4 Model	X Distance (A)	Y Distance (A)	Z Distance (A)	Sum (A)	Product (A^3)	Best Peptide Dock	Best AFB1 Dock
Empty Model	10.463	14.520	11.752	36.735	1785.4	8.4	-10.2
Ritonavir	12.174	18.025	10.071	40.27	2209.9	-5.7	-9
Progesterone	10.491	13.972	11.559	36.022	1694.3	11.7	-9.7
PKT	11.028	15.198	12.042	38.268	2018.3	-5.2	-8.9
PK9	14.528	10.720	11.881	37.129	1850.3	1.3	-9.9

Table 1; CYP3a4 results. The name of each model refers to the ligand that was originally bound in the active site before peptide docking took place. The X, Y, and Z dimensions of the active site are listed for each model of CYP3a4, as are the sum and product of the dimensions and the best docks for both the peptide and AFB1.

The dock of the cyclic peptide with the *"Progesterone"* model of CYP3a4 was the poorest dock of all. This seems to be primarily due to steric effects, since the cyclic peptide can be seen protruding from the active site, unable to fully fit within the model. This is not surprising, as the data in Table 1 shows that the *"Progesterone"* model of CYP3a4 has the smallest product of active site dimensions, indicating the smallest active site. The size of the cyclic peptide seems to have kept it from being able to fully fit inside of the active site. In this model, and all models of CYP3a4 besides *"Ritonavir,"* the cyclic peptide docked into the active site with its disulfide bridge facing the heme group.

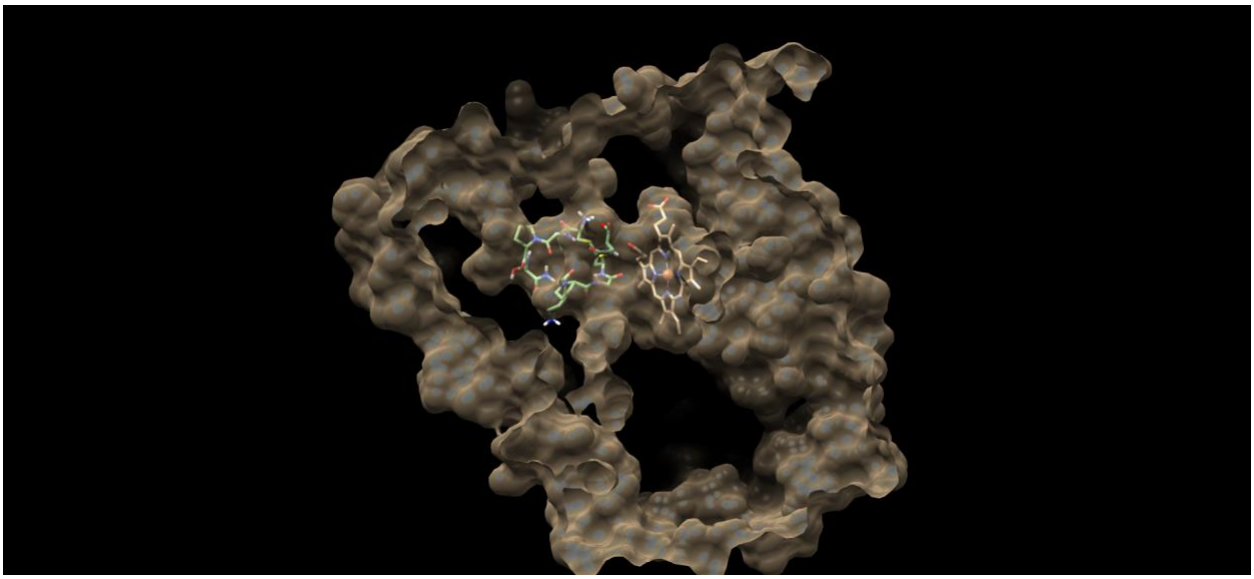

Figure 14; Dock of Cyclic Peptide with Progesterone model of CYP3a4. The lower section of the peptide can be seen jutting out of the active site.

The Ritonavir model of CYP3a4 reported the strongest docking for the cyclic peptide, in addition to the largest product of active site dimensions. This supports the possibility of steric effects being the primary determinant in cyclic peptide docking strength for CYP3a4 models. Compared to the Progesterone model of CYP3a4, the cyclic peptide can be seen entirely fitting within the active site. In contrast to all other models of CYP3a4, after docking the cyclic peptide with the Ritonavir model, the cyclic peptide is oriented with the disulfide bond facing away from the heme group instead of towards it. The Ritonavir model of CYP3a4 was also the only model in which AFB1 was docked near the heme group.

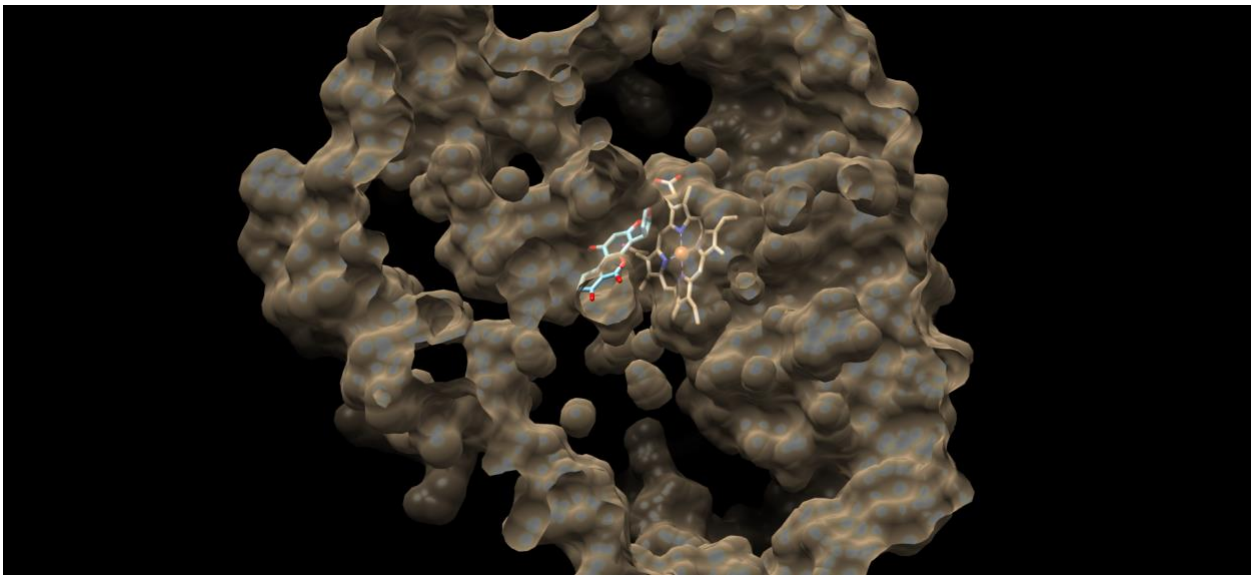

Figure 15; AFB1 docked with Ritonavir model of CYP3a4. AFB1 is bound in close proximity to the heme group in the active site of CYP3a4.

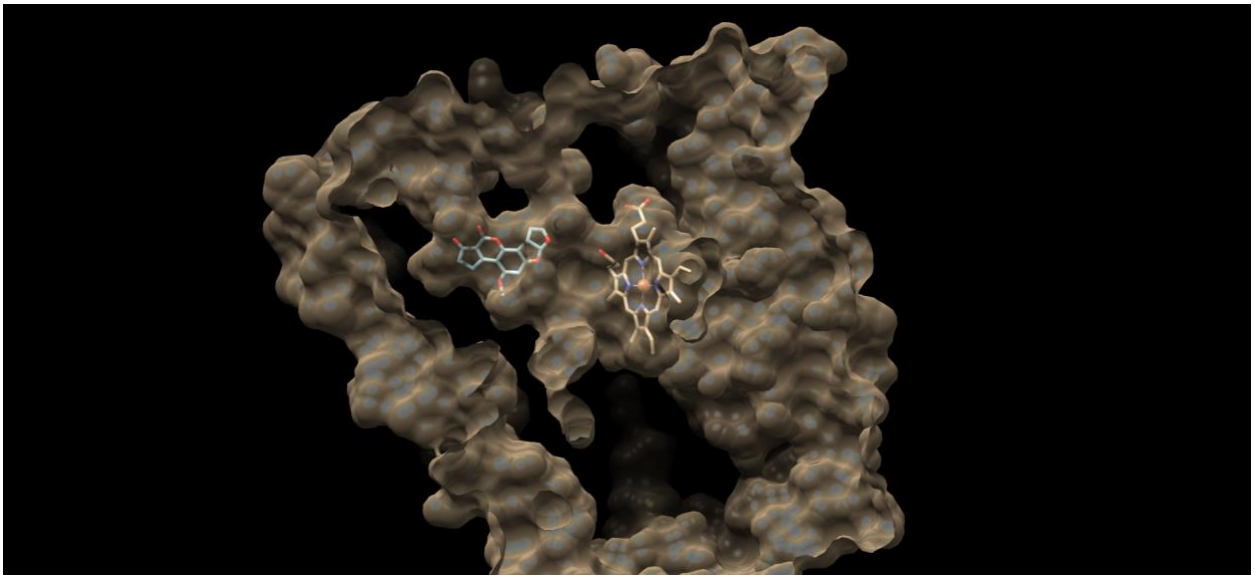

Figure 16; AFB1 docked with Progesterone model of CYP3a4. AFB1 is bound on the opposite side of the active site from the heme group. This orientation was seen in this model, along with all other CYP3a4 models with the exception of the Ritonavir model.

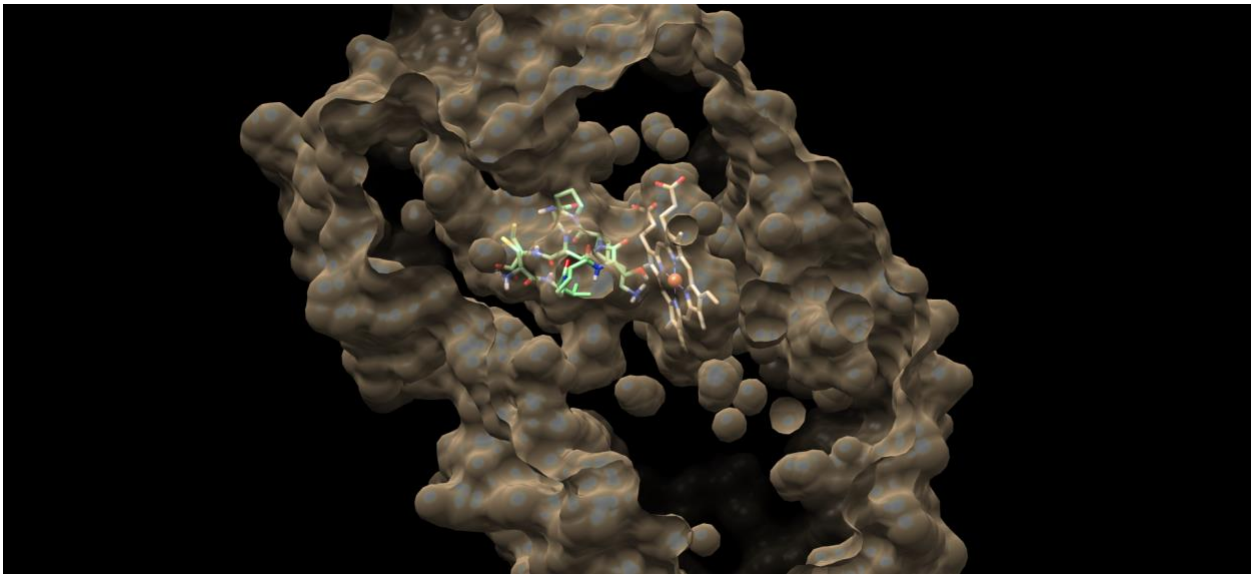

Figure 17; Dock of Cyclic Peptide with Ritonavir Model of CYP3a4.

In addition to CYP3a4, the cyclic peptide and AFB1 were also docked with mAb 2F5. The results from docking the cyclic peptide and AFB1 with mAb 2F5 were organized into a table. The docking strength between the peptide and AFB1 are much closer in value compared to

the various CYP3a4 models. This is not surprising, due to the location of mAb 2F5's active site on the outside of the antibody where steric effects should not play as much of a role in binding, and because mAb 2F5 was the antibody used in the original paper to identify the cyclic peptide as an AFB1 mimitope.

Table 2

Molecule	Best Dock
Peptide	-6.5
AFB1	-7.6

Table 2; mAb 2F5 Cyclic Peptide and AFB1 Dock Results

The mAb 2F5 docks with the cyclic peptide were not very consistent in their orientation within the active site, or even in their selection of the active site for docking. Several of the best docks did not bind to the binding site, but instead to a region of the molecule adjacent to the active site. The best fit, however, did bind correctly to the active site, and overlaps well with the AFB1 best dock. When the best docks of both AFB1 and the cyclic peptide are overlapped, it can be seen that AFB1 is docked in the same region of the mAb 2F5 binding site as the half of the cyclic peptide opposite the disulfide bridge. In other words, the half of the cyclic peptide opposite the disulfide bridge is where a significant overlap with AFB1 is found.

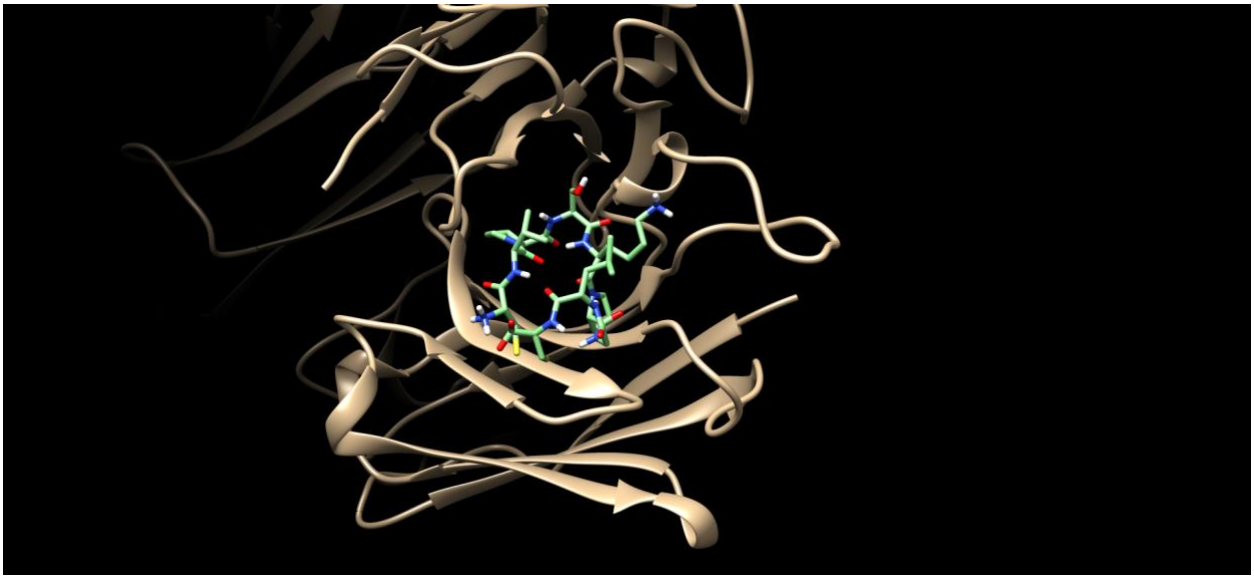

Figure 18; Cyclic Peptide Docked with mAb 2F5.

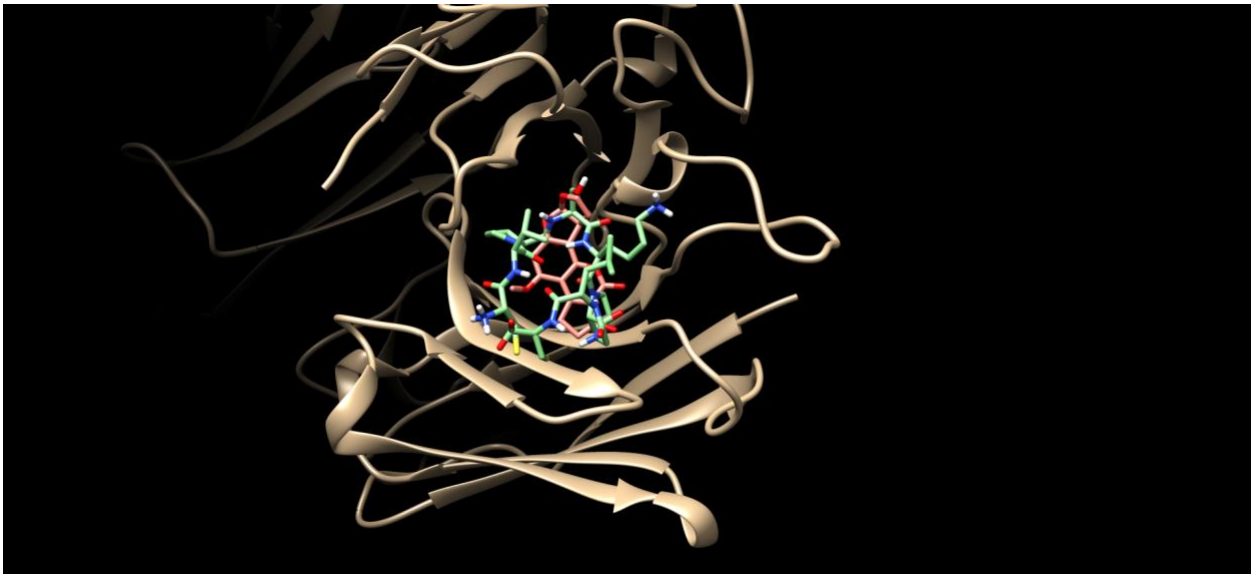

Figure 19; Overlap of mAb 2F5-Docked Cyclic Peptide and AFB1.

Discussion

The measuring of atomic distances to approximate the active site size of CYP3a4 models was successful. The product of the CYP3a4 active site dimensions using the atomic distances previously mentioned seems to be a very effective way of estimating the size of the active site. By using the atomic distances between the selected atoms on opposing sides of the active site, a rectangular approximation of the active site was created, for which the product of the dimensions would be equal to its volume. Though the active site is not rectangular, the approximation was useful and showed a strong correlation with the dock strength of the cyclic peptide (Figure 11). This data indicates that when the cyclic peptide docks with a model of CYP3a4, the primary factor determining binding strength is the active site size. The reason many of the CYP3a4 models docked so poorly was because of the small size of the active site that could not accommodate the entire cyclic peptide. This was not a factor for the docking of AFB1, due to its comparatively small size. AFB1 was able to successfully fit into the active site of every CYP3a4 model.

Docking with mAb 2F5 was less complicated than with CYP3a4 due to the binding site being on the outside of the model and fewer steric constraints being involved. Figure 19 depicts the best docks of the cyclic peptide and AFB1 with mAb 2F5 overlapped with each other. This overlap reveals a general orientation of the cyclic peptide with respect to AFB1 that repeats through different docks between both mAb 2F5 and CYP3a4. In the best dock models, the best overlap consistently shows AFB1 and the cyclic peptide arranged where the disulfide bond of the cyclic peptide is facing away from AFB1, and the majority of the overlap between the two

models is taking place on the side of the cyclic peptide with the Serine residue, opposite the disulfide bridge. This indicates that the structural feature enabling the cyclic peptide to act as an AFB1 mimotope is likely within the half of the molecule opposite the disulfide bridge. This is an observation that lines up with what would be expected. The function of the disulfide bridge, and more generally the reason to use a cyclic peptide as opposed to a linear peptide, could very likely be the reduction of steric interference from the rest of the peptide on the residues relevant for the mimotope function. The cyclization of the peptide better reveals the relevant residues of the peptide and allows for easier binding. Without the disulfide bridge, the peptide may not have been able to bend in the specific ways necessary to bind to CYP3a4 and mAb 2F5 in the ways that it did.

The docks of the cyclic peptide with mAb 2F5 were not very consistent. Only three of the top ten docked models were docked to the canonical antibody binding site, and each of them were docked in a different orientation. The reported strength of every dock was also very similar, with the best dock being a strength of -6.5 and the worst being -5.9. Though this seems to indicate that the docks were very close in energy, a difference of only 0.6kcal/mol, when used to calculate the dissociation constant, is quite a large difference. The dissociaton constant is a value representing how tightly bound a ligand is to a receptor. The lower the number, the more tightly bound the ligand is. Calculating the dissociation constant with a free energy value of -6.5kcal/mol results in an answer of 6.256E-6, while the energy value of -5.9kcal/mol gives an answer of 1.887E-5. Despite how close the free energy values are, the dock that scored -5.9 has a dissociation constant that is more than twice as large as the dock that scored -6.5. This shows that though the free energies of the docks seem similar in value, there is a substantial difference between the docks in terms of their binding strength. The AFB1 docks with mAb 2F5 were much

more consistent. Only two of the top ten docks were located outside of the binding site. In terms of energy, the range for the AFB1 docks with mAb 2F5 was slightly larger, with the best dock being -7.6 and the worst being -6.4 for a range of 1.2. This implies that there may be fewer optimal dock positions for AFB1 with mAb 2F5 than there are for the cyclic peptide.

The results from this experiment provide a good basic framework for understanding the cyclic peptide and its function as an AFB1 mimotope, but there are a couple of further steps that could be taken to learn more. First, a different docking or modeling program could be used. One limitation to this experiment was that the modeling and docking programs used only allowed for movement of the ligand during docking, not of the receptor. This was especially a limitation for this experiment due to the importance of CYP3a4 active site size in the quality of results. If the active site had been able to conform to the ligands during docking, the dock scores would have likely been much better and much more would have been learned about how AFB1 and the cyclic peptide bind to CYP3a4. Second, successive docks could be performed to ensure higher quality and more consistent docks. After the first dock is complete, another dock using the ligand in its first docked position may produce results that are of higher quality than the first round of docking.

This experiment has somewhat succeeded in answering its core questions: by what structural similarities does the cyclic peptide act as a mimotope of AFB1, and how similarly do the two molecules bind to CYP3a4 and mAb 2F5? This question was, to some extent, answered. The docking results show that the cyclic peptide does have similar dock strength to AFB1 when docked with mAb 2F5, though the results of docks with CYP3a4 were inconclusive because of the active sites in the models used being too small to accommodate the cyclic peptide. The analysis of docking results leads to the conclusion that it is likely the half of the cyclic peptide

opposite the disulfide bridge that is responsible for the mimotopic behavior, due to the fact that in all of the best docks, this region of the cyclic peptide was overlapped with the best docks of AFB1. There are, however, still questions that remain unanswered. This experiment did not successfully reveal the specific structural components of the cyclic peptide that cause it to bind similarly to AFB1. It also failed to fully explore the binding interaction between the cyclic peptide and CYP3a4 due to steric constraints in the models used.

Works Cited

Alex P. Wacoo, Deborah Wendiro, Peter C. Vuzi, Joseph F. Hawumba, "Methods for Detection of Aflatoxins in Agricultural Food Crops", *Journal of Applied Chemistry*, vol. 2014, Article ID 706291, 15 pages, 2014. https://doi.org/10.1155/2014/706291

Benkerroum N. (2020). Chronic and Acute Toxicities of Aflatoxins: Mechanisms of Action. *International journal of environmental research and public health*, *17*(2), 423. https://doi.org/10.3390/ijerph17020423

Mukhtar, H., Ma, L., Pang, Q. *et al.* Cyclic peptide: a safe and effective alternative to synthetic aflatoxin B_1-competitive antigens. *Anal Bioanal Chem* **411,** 3881–3890 (2019). https://doi.org/10.1007/s00216-019-01862-7

Sevrioukova, I. F., & Poulos, T. L. (2013). Understanding the mechanism of cytochrome P450 3A4: recent advances and remaining problems. *Dalton transactions (Cambridge, England : 2003)*, *42*(9), 3116–3126. https://doi.org/10.1039/c2dt31833d

Nyenhuis, D. Cytochrome P450 3A4. https://collab.its.virginia.edu/access/content/group/f85bed6c-45d2-4b18-b868-6a2353586804/2/Ch00_Nyenhuis_D_Cytochrome_P450_3A4-_-/Ch00_Nyenhuis_D_Cytochrome_P450_3A4_CYP3A4.html

O. Trott, A. J. Olson, AutoDock Vina: improving the speed and accuracy of docking with a new scoring function, efficient optimization and multithreading, *Journal of Computational Chemistry 31 (2010) 455-461*

UCSF Chimera--a visualization system for exploratory research and analysis. Pettersen EF, Goddard TD, Huang CC, Couch GS, Greenblatt DM, Meng EC, Ferrin TE. *J Comput Chem.* 2004 Oct;25(13):1605-12.

Aflatoxin B1 Model acquired from http://www.chemspider.com/Chemical-Structure.162470.html

PDB ID: 3idg
Crystallographic Definition of the Epitope Promiscuity of the Broadly Neutralizing Anti-Human Immunodeficiency Virus Type 1 Antibody 2F5: Vaccine Design Implications. Steve Bryson, Jean-Philippe Julien, Rosemary C. Hynes, Emil F. Pai. Journal of Virology Oct 2009, 83 (22) 11862-11875; DOI: 10.1128/JVI.01604-09

PDB ID: 4D7D
Structure-Based Inhibitor Design for Evaluation of a CYP3A4 Pharmacophore Model. Parminder Kaur, A. Richard Chamberlin, Thomas L. Poulos, and Irina F. Sevrioukova. Journal of Medicinal Chemistry 2016 59 (9), 4210-4220. DOI: 10.1021/acs.jmedchem.5b01146

PDB ID: 4D75
Structure-Based Inhibitor Design for Evaluation of a CYP3A4 Pharmacophore Model. Parminder Kaur, A. Richard Chamberlin, Thomas L. Poulos, and Irina F. Sevrioukova. Journal of Medicinal Chemistry 2016 59 (9), 4210-4220. DOI: 10.1021/acs.jmedchem.5b01146

PDB ID: 5A1R
Anion-Dependent Stimulation of CYP3A4 Monooxygenase. Irina F. Sevrioukova and Thomas L. Poulos. Biochemistry 2015 54 (26), 4083-4096. DOI: 10.1021/acs.biochem.5b00510

PDB ID: 5VC0
High-Level Production and Properties of the Cysteine-Depleted Cytochrome P450 3A4. Irina F. Sevrioukova. Biochemistry 2017 56 (24), 3058-3067. DOI: 10.1021/acs.biochem.7b00334

PDB ID: 1TQN
The Structure of Human Microsomal Cytochrome P450 3A4 Determined by X-ray Crystallography to 2.05-Å Resolution. Yano J. K., Wester M. R., Schoch A. G. Journal of Biological Chemistry 2004 279 (37) 38091-38094. DOI: https://doi.org/10.1074/jbc.C400293200

Molecular graphics and analyses performed with UCSF Chimera, developed by the Resource for Biocomputing, Visualization, and Informatics at the University of California, San Francisco, with support from NIH P41-GM103311.